Received: 16 October 2016 | Accepted: 1 June 2017

DOI: 10.1111/jace.15038

ORIGINAL ARTICLE

Microstress in the matrix of a melt-infiltrated SiC/SiC ceramic matrix composite

Bradley L. Wing | **John W. Halloran**

Material Science and Engineering, University of Michigan, Ann Arbor, Michigan

Correspondence
Bradley L. Wing, University of Michigan Material Science and Engineering, Ann Arbor, MI.
Email: wingbrad@umich.edu

Funding information
General Electric

Abstract

Microstress in the SiC: Si matrix of a ceramic matrix composite (CMC) has been characterized, using Raman spectroscopy. The matrix of the composite was manufactured using liquid melt infiltration, and has about 20% unreacted free silicon. During the processing of the composite, the unreacted free silicon expands 11 vol % when transforming from liquid to solid. This crystallization expansion creates compressive microstress in the silicon phase of the matrix, which ranges from 2.4 to 3.1 GPa, and tensile microstress in the SiC of the matrix which ranges from 0.24 to 0.75 GPa. The microstress varies significantly with position, following a normal distribution.

KEYWORDS
composites, Raman spectroscopy, silicon, silicon carbide

1 | INTRODUCTION

Fiber-reinforced ceramic matrix composites (CMCs) are important for many applications to reduce weight[1,2] and increase temperature capabilities.[3] Composites with silicon carbide fibers and a silicon carbide matrix (SiC/SiC) have been identified as a key class of CMCs for aerospace applications. The matrix SiC can be produced by infiltration and pyrolysis of a SiC preceramic polymer,[4,5] by chemical vapor infiltration,[6,7] or by melt infiltration.[8,9] For this paper, we consider composites reinforced with SiC fibers with a reaction bonded silicon carbide (RBSiC) matrix produced by infiltration of molten silicon into a carbonaceous preform (MI SiC/SiC CMC). This MI SiC/SiC composite has a nearly pore free matrix, which contains about 20 vol % unreacted free silicon. The matrix is thus a two-phase mixture of SiC and free silicon. At the melt infiltration processing temperature, there is residual liquid free silicon after the reaction bonding process. Upon cooling, the liquid silicon crystallizes. Silicon is unusual in that it expands during crystallization by about 11 vol%, which corresponds to a linear crystallization expansion strain, ε_{CES}. of about 0.037. This crystallization expansion strain of the silicon phase causes a smaller expansion of the Si:SiC matrix. This matrix expansion, if constrained, can give rise to complex, multiaxial residual stress in the matrix on a length scale comparable to the scale of the grain size. This may contribute to the matrix residual stresses which influences matrix cracking in MI SiC/SiC CMC as seen by Morscher et al.[10,11] and Appleby.[12]

On a very fine scale, the crystallization expansion of the silicon phase is constrained by the surrounding SiC matrix grains. Thus we anticipate microstresses in the Si:SiC matrix, with the expanding Si phase experiencing compressive microstress, and the constraining SiC phase experiencing tensile microstress. As was shown in a previous paper,[13] the stresses that develop from crystallization expansion in RBSiC are much larger and more consequential than stresses that are formed from the thermal expansion mismatch of the two-phase mixture. The spatial range of these microstresses would be comparable to the matrix grain size, which is a few micrometers. Recently, we reported the characterization of microstresses in monolithic reaction bonded SiC.[13] We characterized the microstresses at the surface from shifts in the Raman Spectra for the silicon phase and the SiC phase. Here we report on the hydrostatic component of the complex stress tensor from the Raman measurements at each location in the matrix SiC and matrix free silicon in

© 2017 The American Ceramic Society

the matrix of a commercial MI SiC/SiC composite. It is important to note, in this paper we do not discuss the relaxation of stress during processing of the composite. This is an important topic for the processing and use of the composite and will be discussed in a future paper.

2 | METHODS

2.1 | Material

We examined the commercial MI SiC/SiC CMC manufactured by GE Aviation, HiPerComp™ (Cincinnati, OH).[9,14] This material is a continuous fiber reinforced composite produced by melt-infiltration using silicon carbide fibers with a boron nitride (BN) interphase coating. The architecture of this composite is a cross-ply laminate of eight plies of uniaxial fibers with a [0/90]2s layup, resulting in a through-thickness of ~2 mm. The samples represented in this paper are all cut from a single panel using a slow-speed diamond saw. Each sample is approximately 10 mm×25 mm×2 mm.

The free silicon in the Si:SiC matrix was determined by quantitative XRD, using the method of standards. Pulverized samples of the composite were combined with known amounts of powdered silicon. We then compared the integrated intensities of the three silicon peaks ((111), (220), and (311) peaks) and the four SiC peaks (silicon peaks and (101), (102), (103), (104), and (110) α-SiC peaks). The β-SiC (111) and (220) peaks are close to the α-SiC peaks (102) and (110) peaks, so this procedure captures both alpha-and beta-silicon carbide. The total intensity of silicon peaks and SiC peaks were determined for mixtures of pulverized composite with added powder silicon. This included the amount added as well as the amount of silicon in the CMC. We are then able to determine the linear relationship between the intensity ratio and the exact amount of free silicon to within ±5 vol%.

2.2 | Microstress measurement

We used Raman spectroscopy to measure the residual microstress in the matrix RBSiC of this CMC. Raman spectroscopy has been shown effective in measuring the residual microstress in both silicon[15–17] and SiC.[18–21] For a Raman active material, there is a characteristic wavenumber associated with the bonding to particular Raman modes. A stress in the material causes the characteristic wavenumber of the Raman mode to shift, with shift to a lower wavenumber for tension and shift to a higher wavenumber for compression. The difference between the characteristic wavenumber and the shifted wavenumber (Δω) can be directly related to the stress (σ) applied to the material through the Raman coefficient, R:

$$\Delta\omega = R\sigma \tag{1}$$

We will use Raman coefficients from the literature. For silicon, we use the $q\approx 0$ optical phonon Raman peak at 520 cm^{-1}, for which R_{Si}=1.88±05 cm^{-1}/GPa as determined by Anastakakis.[17] It is worth noting that the silicon used in this study is not considered pure. However, the Raman signals followed the form a Lorenzian peak. It has been shown that dopant levels high enough to affect the characteristic peak location of silicon will also form a Breit-Signer-Fano (BWF) peak shape. The silicon peaks we observed do not have BWF shape, and there, we will use the Raman coefficient for pure silicon to infer the apparent stress values from the shifts.[22] For polycrystalline SiC, we use the full triplet transverse optic (TO) phonon mode Raman peak at 797 cm^{-1}, for which used 3.53±0.21 cm^{-1}/GPa as determined by DiGregorio.[20] This has been shown to be consistent for α and β-SiC.[23] We confirmed that the peak shifts correlated with applied stresses using the flexural apparatus reported by Stadelmann et al.[23]

The values of the shifts (Δω) are the results of subtracting the known, unstressed peak locations from the measured stressed peak location. As these peaks are broad some uncertainty is introduced. The uncertainty is larger in the SiC because the transverse optic phone around 797 cm^{-1} has to be fit as a triplet and is only about 20% as intense as the simple silicon peak at 520 cm^{-1}.

The peak locations were measured using a custom system set up with the assistance of Dr. Francis Esmonde-White.[24,25] Details of the system are reported elsewhere.[13,26] Briefly, we used a 532 nm green laser, fed into a collimator via a fiber optic cable, and refracted toward the Nikon Eclipse ME600L microscope (Nikon Instruments inc., Melville, NY) using a dichroic filter. The laser travels through the optics of the microscope and is incident on the sample with a spot size of 20 μm, which ensures that hundreds of SiC and silicon matrix grains are sampled at every position. Raman excited photons pass back through the microscope optics and go through two filters to remove the reflected 532 nm wavelength. The filtered, collimated photons are separated based on energy levels with the HoloSpec VPT spectrograph and are read to the computer with the Newton EM CCD. We used a two-system calibration method; the CCD using an argon light emission spectrum and the laser separately using acetaminophen.

Fourteen samples were analyzed. Each sample was examined as-manufactured. All samples were polished to a 1 μm finish with a nonaqueous solution. Twenty measurements were taken from the surface of each sample. Care was taken to ensure that the spectra were collected from a region of matrix at least 20 μm from a fiber, since fluorescence from the BN coating on the fiber interfered with the Raman spectra. Spectra were collected from 280 locations,

providing pairs of microstress measurements for the silicon and SiC phases. Peak fitting was done manually using Origin 9.1 software. As was done in the previous study, all silicon peaks were fit easily with a Lorenzian curve and the SiC peaks were fit with a Gaussian curve. The error in determining the peak location is taken into account in the error measurements presented in this paper. Error bars were calculated using the uncertainty obtained from the literature as well as the uncertainty of the peak location calculated based on a 95% confidence. The two uncertainties were considered independent and the reported error values were compiled using the variance formula. The measured microstress in the 20 locations was averaged together to determine the microstress value reported for each individual sample.

3 | RESULTS

3.1 | Microstructure and free silicon

A polished cross section appears in Figure 1A. Here we see alternating lamina containing longitudinal SiC fibers (visible by their polished cross section or by the long voids from fiber pulled out during polishing) and lamina with transverse fibers (visible from the round fiber cross-sections). Notice that each fiber-containing ply is about 200 μm thick, and the plies are separated by a layer of RBSiC matrix that is about 100 μm thick. The area of concern is the thick center layer that contains only the matrix. All measurements were taken from this region to avoid the florescence of the BN coatings, as well as for consistency.

It is difficult to obtain clear contrast in the SEM between the matrix SiC and the free silicon, so a polished sample was etched with potassium hydroxide to dissolve the silicon. A secondary electron image of the microstructure in this region can be seen in part B of Figure 1. The voided regions represent where the silicon was during the measurements. Etching away the silicon was done only for imaging purposes. No Raman measurements were taken on samples with silicon etched out.

The free silicon is known to be an interconnected phase.[27] The size of the silicon areas are on the order of a few hundred nanometers. The individual matrix SiC grains are not resolved in Figure 1B, but from the outline of the etched silicon, showing the spacing of the silicon phase, it is possible to infer that the SiC grain size is on the order of 1 μm, which is similar to what was reported for this material by Corman and Luthra[9] and Dunn.[27]

Raman spectra were collected in the central matrix region, as illustrated by the box in Figure 1A. Reflected light images of four representative locations are shown in Figure 2A-D. The spots where the spectra were collected are shown as black rings (~20 μm in diameter), and the

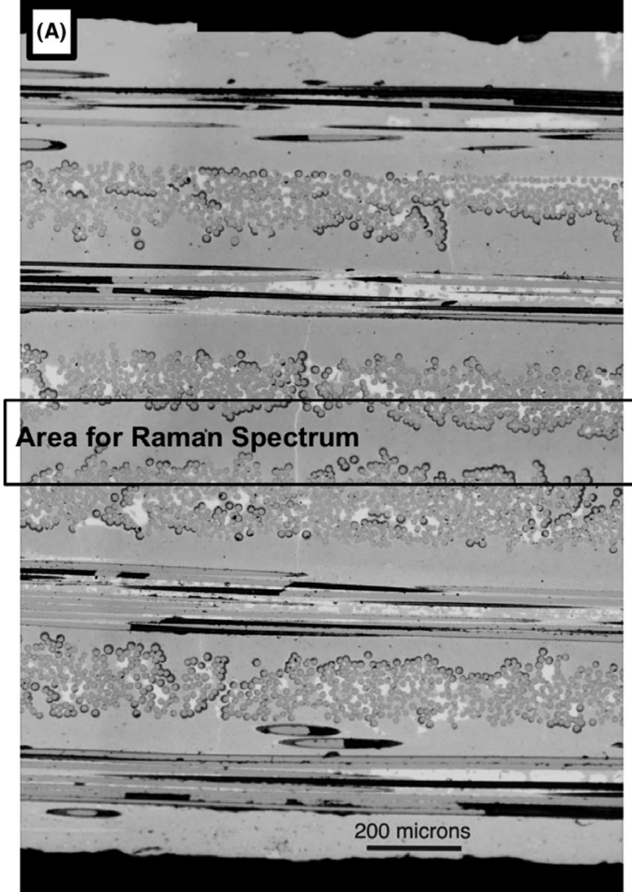

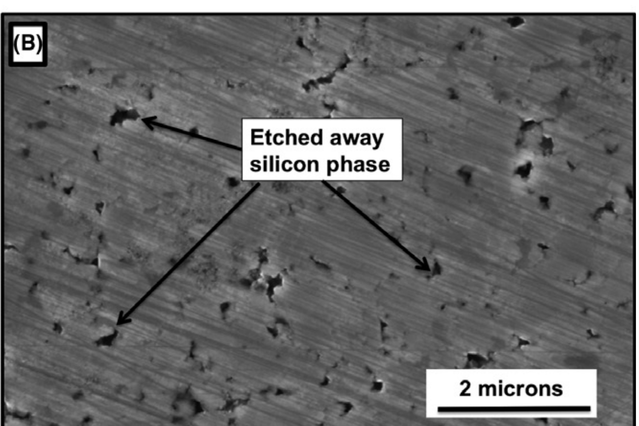

FIGURE 1 Image A is an optical image of the 8-layer uniaxial composite. The circles are cross-sections of the 90 fiber going in and out of the page. The horizontal lines are fibers in the 0 direction, perpendicular to the 90 fibers. Image B shows a secondary electron image of the RBSiC matrix after the silicon has been etched out using KOH

mottled contrast indicates the darker SiC and brighter free silicon. Since the SiC grains are approximately 1 μm, and the silicon grains are much smaller, the 20 μm spot size shown in Figure 2A-D is sampling multiple grains of both phases. Spectra are collected from ~300 SiC grains per scan, which we can presume have random crystallographic

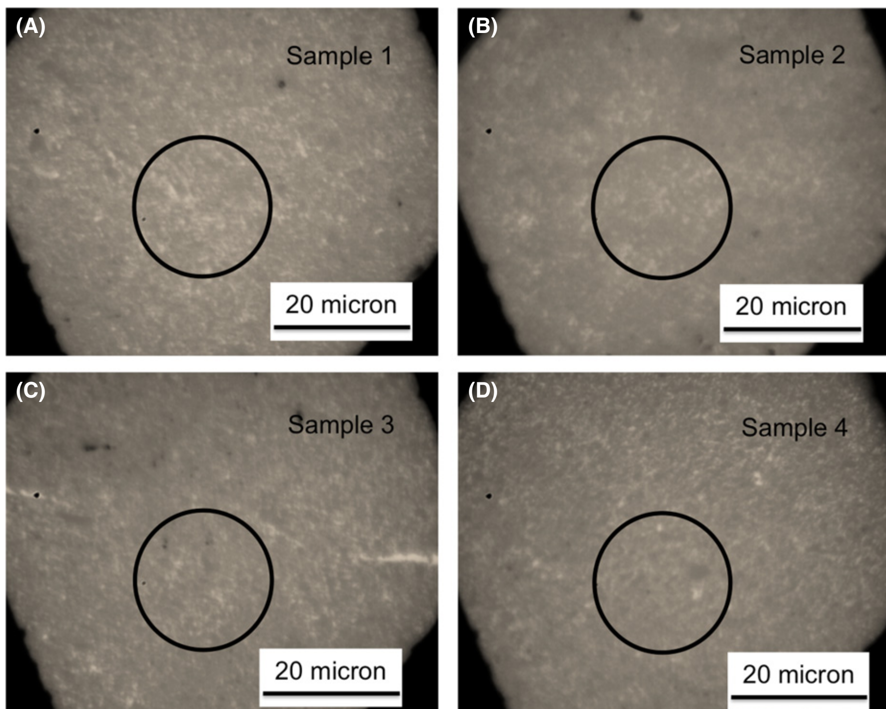

FIGURE 2 Reflected light optical images of four different positions in four different samples. The black circles indicate the position of the light source [Color figure can be viewed at wileyonlinelibrary.com]

orientation. The free silicon phase, present as an interconnected phase a few hundred nanometers thick between the SiC, crystallizes as single crystal domains several micrometers in size.[26] The 20 μm spot size samples many of these so we treat the free silicon as random polycrystals.

In Figure 3A, we provide the full Raman spectra for each of the regions pictured in Figure 2A-D. Each individual spectrum contains the $q \approx 0$ phonon peak for silicon (near 520 cm^{-1}) as well as the TO peak for SiC (near 797 cm^{-1}). The silicon peaks for the four locations are shown in detail in Figure 3B. The vertical black line shows the position of the unstressed $q \approx 0$ phonon peak at 520 cm^{-1}. The measured silicon peaks are sharp and well defined. The red dotted line indicates the curve fit used to determine the peak position. At all four locations, the Raman peak shifts to higher wavenumber, indicating a compressive stress in the silicon.

Similarly, we show the TO SiC peaks for each position Figure 3C. Due to the triplet splitting, the SiC TO peak is much broader. The SiC peaks are less distinct, but peak fitting shows that they are shifted to lower wavenumber, consistent with tensile stresses in the silicon carbide.

The peak positions and the stresses inferred from the wavenumber shift $\Delta\omega$ for the spectra collected from these four representative locations can be seen in Table 1. The error limits in the calculated microstress, amounting to 0.1-0.2 GPa, comes from the uncertainty in the peak positions from the peak fitting. To establish the repeatability of the Raman spectra themselves, at several locations the spectra were collected three times. The peak positions obtained by fitting the spectra were within the uncertainty of the peak fit, i.e., within 0.2 cm^{-1} for the silicon and within 0.7 cm^{-1} for the SiC.

The variability in the measurement itself is not known, but we believe this evidence that the local residual microstress is variable. We will interpret this as if the microstress values were locally varying. For the silicon, with a simple peak, the peak position varies by about 6% between the four locations. The average inferred compressive stress for these four positions is about 2.8 GPa, varying from 2.4 to 3.1 GPa. The magnitude of the tensile stress inferred for the SiC shows about the same magnitude of variability. The average tensile stress for these four locations is 0.54 GPa, and it varies from 0.24 to 0.75 GPa.

3.2 | Position to position variation

Figure 4 shows the apparent values of compressive stress in the silicon and apparent tensile stress in the SiC inferred from the Raman shifts for the 20 positions of a single sample. We have plotted the data as pairs of points (σ_{Si} and σ_{SiC}) calculated from the $\Delta\omega_{Si}$ and $\Delta\omega_{SiC}$ from fitting the spectra at each position. It is convenient to present these data as plots with tensile stress in SiC in the vertical axis and compressive stress in the free silicon in the horizontal axis, so that a point can represent each pair.

For this single sample, we see variation in the apparent tensile stress in the SiC phase from nearly 0 GPa up to about 1.4 GPa. For the compressive stress in the silicon phase, we see a variation from about 2.5 to 3.5 GPa. The silicon shows slightly lower variation than what is observed in the SiC phase for this sample. The error bars in Figure 4

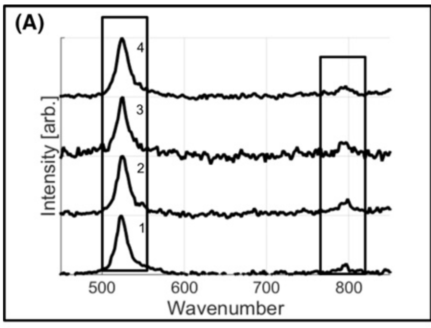

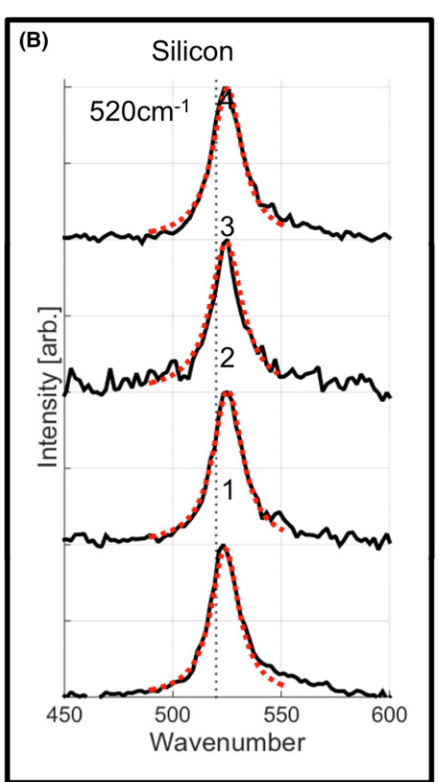

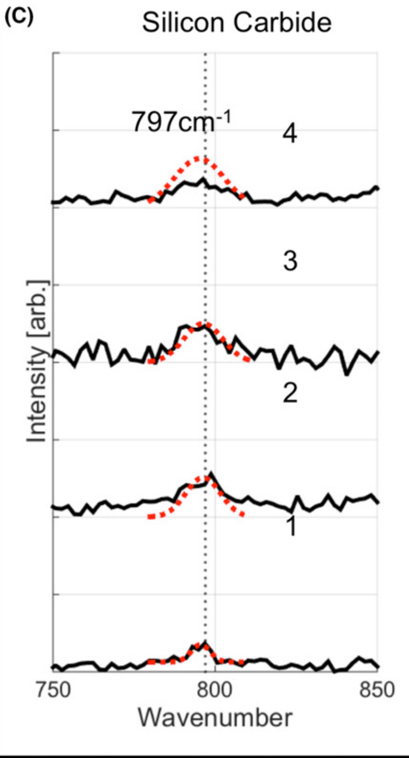

FIGURE 3 In part A, there are the four spectra from the images shown in Figure 1.1. We have shown the silicon peaks for the four images in part B. The black vertical line shows the location for the unstressed silicon at 520 cm^{-1} and the red dotted line shows the fit using the Origin software. In part C, we have the SiC peaks for the four positions. The black vertical line indicates the unstressed TO peak for SiC at 797 cm^{-1} and the red dotted lines indicate the fit using the Origin software [Color figure can be viewed at wileyonlinelibrary.com]

TABLE 1 The peak positions and resulting microstress values for the locations shown in part A of Figure 2

Sample	Silicon peak position (cm^{-1})	SiC peak position (cm^{-1})	Silicon compressive microstress (GPa)	SiC tensile microstress (GPa)
1	524.02±.20	795.54±.51	2.39±.12	0.41±.15
2	525.27±.26	796.12±.67	3.14±.15	0.25±.19
3	524.34±.28	796.31±.49	2.58±.17	0.19±.14
4	525.03±.21	794.32±.74	2.99±.12	0.75±.21

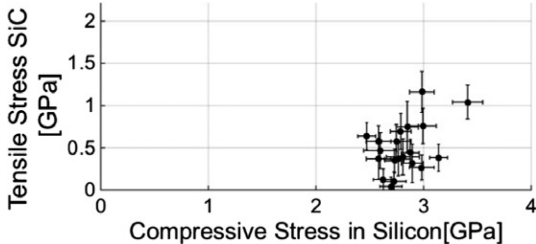

FIGURE 4 Each residual microstress measurement for a single sample with error bars for the uncertainty of each measurement. Each point represents the pair of stresses in the silicon and silicon carbide at that location

represent the uncertainty in the peak fitting. The error in the compressive stress in the silicon phase averages out to be about ±0.1 GPa. The average error in the SiC phase is about double that of the silicon phase, ±0.2 GPa. This error is consistent for all the samples in this study.

In Figure 5 we show the combined results for 280 locations in fourteen separate specimens, all cut from a single panel. In this case, we omit the error bars for clarity. In this figure, we see that there is significant variation from one location to another. We could find no systematic variation with position in the composite panel, or with proximity to fiber-containing tows. Rather this appears to be statistical variation in the magnitude of the microstress. We

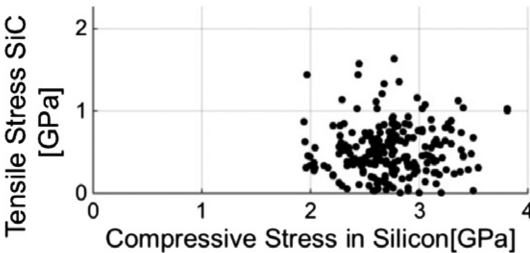

FIGURE 5 Plot of the measured compressive stress in silicon and tensile stress in SiC phases at every position for all samples. Error bars omitted for clarity

have a large confidence in the stress measured in the silicon phase since the peaks have high intensity and are narrow. Therefore we know that the stress is different from location to location. In the SiC phase, we are less confident because the low intensity and broad peaks are more difficult to fit. However, both the silicon and SiC phases show a normal distribution with very similar standard distributions, providing more confidence in the tensile microstress measured in the SiC phase.

Figure 6 displays the frequency distributions for compressive microstress values in the silicon and tensile microstress values in the SiC phase. Superimposed on the observed frequency distribution normal distribution function, which can give an estimate of the mean and standard deviation. The mean value for the compressive microstress in silicon is 2.72 GPa with a standard deviation of 0.36 GPa, for a coefficient of variation of about 13%. The distribution of tensile microstress in the SiC has a mean around 0.50 GPa and a standard deviation of 0.33 GPa. Because the mean is smaller, the coefficient of variation for the SiC microstress is about 66%. Note that Stadelmann et al[23] also reported a normal distribution for the thermoelastic microstress in the SiC phase in the ZrB_2–SiC systems, with a coefficient of variation also around 50%-66%.

3.3 | Sample to sample variation

Figure 7 shows the average microstress values determined for each of the 14 samples of the CMC (black points). The gray X shows the overall mean microstress value from all of the positions examined. The open circle is the value estimated from a Kingery-Turner model, modified to consider crystallization expansion strain instead of thermoelastic strain, without stress relaxation, which provides and estimate of the upper limit for the microstress.[13]

We see that averaging all of the microstress measurements within each sample greatly reduces the apparent variation in the system. The unrelaxed Kingery-Turner estimate is about 20% larger than the measured compressive microstress in the silicon, and about 40% larger than the tensile microstress inferred in the silicon carbide phase. This is

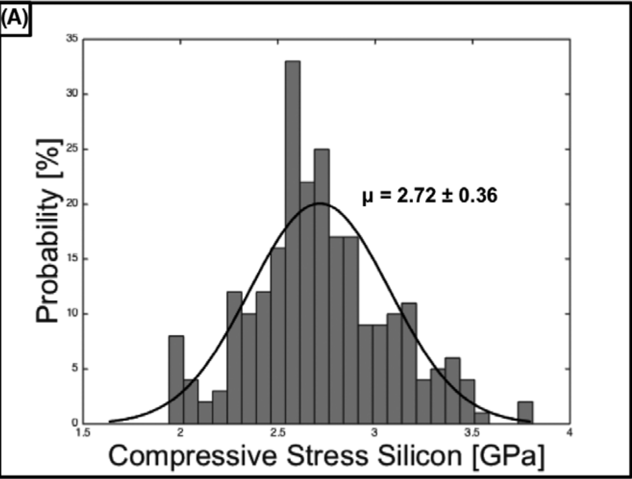

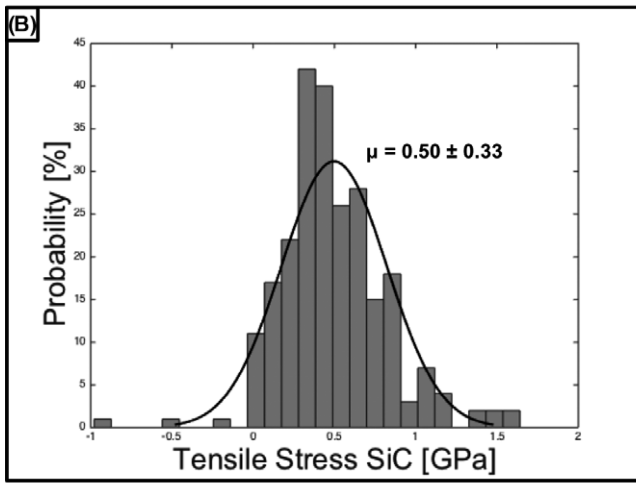

FIGURE 6 Normal distribution curves for the compressive stress in silicon (A) and the tensile stress in SiC (B)

most likely due to relaxation, which will be discussed in detail in the following sections.

4 | DISCUSSION

4.1 | Estimation of microstress before relaxation

To estimate the upper limit of the residual stresses, we consider simple models without relaxation.

4.1.1 | Microstresses from thermoelastic mismatch

Thermal microstresses arising from thermal expansion differences are well known. We can estimate the thermoelastic microstress that would develop from a thermal expansion mismatch using the simple model from Kingery[28] and Turner.[29] This model relates the stress in each phase to the difference between the thermal expansion of that phase and the two-phase assemblage:

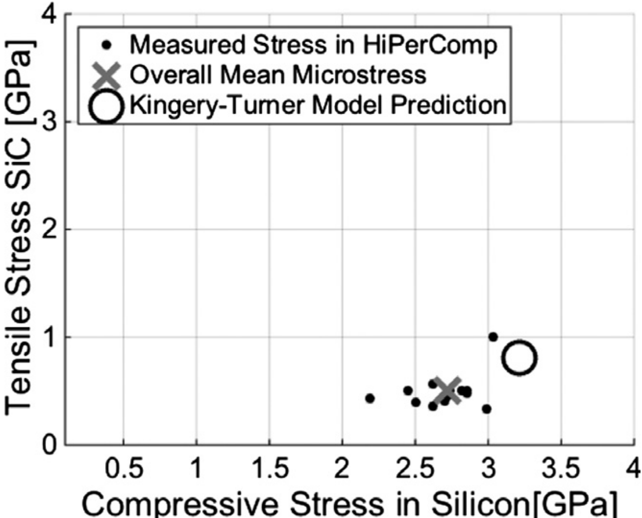

FIGURE 7 Measured microstress values from RBSiC materials using Raman spectroscopy. Black points indicate the average microstress for each sample. The gray "X" indicates the overall mean value for all of the samples. The circle shows the Kingery-Turner model prediction

$$\sigma_i = (\alpha_r - \alpha_i)\Delta T K_i = \Delta\alpha\Delta T K_i, \tag{2}$$

where σ_i is the microstress in the particular phase, α_i is the coefficient of thermal expansion for the phase of interest, K_i is the bulk modulus for the phase, ΔT is the temperature gradient, and α_r is the net expansion coefficient of the two-phase assemblage, described by:

$$\alpha_r = \frac{\alpha_1 K_1 V_1 + \alpha_2 K_2 V_2}{K_1 V_1 + K_2 V_2} \tag{3}$$

In Equation 3 α is the coefficient of thermal expansion, V is the fraction of the phase, and K is again the bulk modulus. The 1 and 2 designations are for the two phases being examined. As reported elsewhere,[13,26] we can estimate the thermoelastic stresses for the silicon and SiC from cooling from the freezing point of the silicon to room temperature. Using literature values for the temperature-dependent thermal expansion of SiC[30] and of silicon,[31] and approximating the bulk moduli with the room temperature bulk modulus values of 100 GPa for silicon and 200 GPa for SiC, we expect a compressive microstress of 103 MPa in silicon and a tensile microstress of 26 MPa in SiC with a 20% volume of silicon. These are of the correct sense, but are much lower than what we infer from Raman spectroscopy. These thermoelastic stresses are on the order of what is observed between the fiber and the matrix in SiC/SiC CMCs.[32]

4.1.2 | Microstress from crystallization expansion strain

As presented in more detail before,[13] we propose that the expansion of the silicon phase when it crystallizes can be treated similarly to thermal expansions mismatch, so that we can model crystallization expansion stresses in analogy to thermoelastic microstresses. Assume that the liquid silicon is trapped in the SiC matrix, and cannot excape when it crystallizes. A volumetric expansion of the silicon phase of 11% corresponds to a linear expansion strain ε_{CES} that is about a third of 0.11, or ε_{CES}=0.037. The expansion of the silicon phase is constrained by the surrounding SiC phase. The Si:SiC matrix expands with the SiC in tension and silicon in compression.

We express the strain in the two-phase mixture in similarly to Equation 3 as:

$$\varepsilon_{Si-SiC} = \frac{\varepsilon_{CES} K_{Si} V_{Si}}{K_{Si} V_{Si} + K_{SiC} V_{SiC}} \tag{4}$$

And substitute this into Equation 2 to estimate the microstress in silicon carbide and silicon from the crystallization expansion strain:

$$\sigma_{SiC} = \varepsilon_{Si-SiC} K_{SiC} = \frac{\varepsilon_{CES} K_{Si} V_{Si}}{K_{Si} V_{Si} + K_{SiC}(1 - V_{Si})} K_{SiC} \tag{5}$$

$$\begin{aligned}\sigma_{Si} &= K_{Si}(\varepsilon_{Si-SiC} - \varepsilon_{CES}) \\ &= K_{Si}\left(\frac{\varepsilon_{CES} K_{Si} V_{Si}}{K_{Si} V_{Si} + K_{SiC}(1 - V_{Si})} - \varepsilon_{CES}\right)\end{aligned} \tag{6}$$

This very approximate model does not consider relaxation and so would predict the upper limit. From Equation 5, we expect the silicon phase to have a compressive microstress on the order of 3.2 GPa with a silicon volume of 20%. Assuming the same silicon volume, Equation 6 suggests a tensile stress of 0.8 GPa.

The average measured values of the microstresses are about the same magnitude, but 20%-40% lower than the maximum value predicted from an unrelaxed Kingery-Turner model. We can see that the modified model provides a good reference for the magnitude of stress measured in the matrix of the composite material. All of the compressive stresses in the silicon phase and nearly all of the tensile stresses in the SiC phase show a lower magnitude than what the model would suggest. This is most likely due to some level of relaxation, which is not taken into account in this model. During processing of the composite, it is likely that some of the residual stress is able to relax.

4.1.3 | Relaxation mechanisms

The model presented here is meant to inform how the residual stress in the CMC is created. In it's current state, the model is not meant to predict values of residual microstress in future CMCs. All of the measurements provided in this study have at least two types of relaxation: (i) relaxation during processing and (ii) relaxation due to sample

preparations. We will briefly discuss these relaxation mechanisms here, but each requires it's one scope of work, which is outside the bounds of this paper.

Since the material in question is processed at high temperatures, it is reasonable to assume some type of relaxation occurs during manufacturing. The silicon is liquid when introduced to the carbon in the melt step of processing. Although the processing conditions are unknown to the authors, we can assume that some type of relaxation would occur during cool down of the CMC. In a future publication, we will consider time and temperature dependence of the stress state. This is important in understanding how the CMC will be affected in use at temperature.

Furthermore, each measurement was taken on a cut and polished surface. The act of cutting the sample removes any stress state perpendicular to the surface. Assuming a small Poison relaxation, the stress state of the in-plane directions should be largely unaffected. This would imply that the hydrostatic stress state at the immediate surface is two-thirds that of the uncut stress state. However, the bulk material will still maintain the original stress state. The functional form for which the stress state changes based on the distance from the cut surface is unknown. Since the green laser used can penetrate the SiC up to a full grain, we have no way of estimating just how much relaxation to assume from the cut surface without knowing the functional form of the relaxation.

4.2 | Position to position variation

This level of variation is far greater than what was examined in the previous study of the monolithic RBSiC materials.[13] In the case of the monolithic materials, the only interaction we need concern ourselves with is the expansion of the silicon against the SiC. Therefore, the two-phase mixture has no other boundary conditions outside the two phases.

In the case of the composite, the microstress measured is again due to the crystallization expansion of the silicon against the stiff SiC phase. However, the composite has other components that can affect the local microstress. Besides the SiC phase in the RBSiC matrix, which constrains the expanding silicon, the composite also has a very strong SiC fiber and a very weak boron nitride (BN) debond coating which varies significantly in thickness throughout the composite. These two elements will therefore impact how the microstress develops in the immediate vicinity of the fiber. These effects will diminish as a function of distance from the fiber, but it is unknown at this time what length scale is necessary to mitigate the effects of the stiff fibers and weak BN coatings on the microstress measured in the silicon and SiC phases.

There is significant variation measured in position to position for each of the samples. This variation reduces nicely in Figure 7 where each point indicates the average of all the measured microstresses in a single sample. This begins to resolve that different specimen may in fact have different stress states due to processing conditions. Furthermore, the variation in microstress measurement from position to position may be a result of localized variation in the processing parameters and not due to the measurement technique.

5 | CONCLUSION

We discovered large residual compressive microstresses in the silicon phase and large residual tensile microstresses in the SiC phase in the matrix of an SiC fiber composite with a matrix of silicon and SiC made by melt infiltration. In the free silicon phase, we measured an average of 2.7 GPa of compression and in the SiC phase, we measured an average of 0.5 GPa of tension. The magnitude and sign of the microstresses measured are consistent with the crystallization expansion of silicon being the cause of the microstress. The maximum expected magnitude of the microstress was estimated with a modification of the Kingery-Turner model, neglecting relaxation. The observed microstress is 20%-40% smaller than the value estimated from the model.

We observed significant variation in the measured microstress from position to position among all of the samples testing. The variation follows a normal distribution in both phases examined. We attribute the variation to the complexity of the microstructure in the composite that the monolithic materials do not have.

ACKNOWLEDGMENT

We thank Professor Michael Morris of the University of Michigan for access to his Raman facilities, and Dr. Francis Esmonde-White for his assistance. We thank Elizabeth Getto for her assistance in providing SEM images used in this manuscript. We thank R. Stadelmann and N. Orlovskaya for access to their flexural/Raman apparatus at the University of Central Florida. This work was funded by GE Aviation under a grant from the University Strategic Alliance.

REFERENCES

1. Naslain RR. SiC-matrix composites: non-brittle ceramics for thermo-structural applications. *Int J Appl Ceram Technol*. 2005;2:75-84.
2. DiCarlo JA, Yun HM, Morscher GN, Bhatt RT. SiC/SiC Composites for 1200°C and Above. In: Bansal NP, ed. *Handbook of Ceramic Composites*. Dordrecht, the Netherlands: Springer; 2005:77-98.
3. Bansal NP, Lamon J, eds. *Ceramic Matrix Composites: Materials, Modeling, and Technology*. Hoboken, NJ: Wiley; 2015.

4. Colombo P, Mera G, Riedel R, Soraru GD. Polymer-derived ceramics: 40 years of research and innovation in advanced ceramics. *J Am Ceram Soc*. 2010;93:1805-1837.
5. Takeda M, Kagawa Y, Mitsuno S, Imai Y, Ichikawa H. Strength of a Hi-nicalon™/silicon-carbide-matrix composite fabricated by multiple polymer infiltration-pyrolysis process. *J Am Ceram Soc*. 1999;82:1579-1581.
6. Probst KJ, Besman TM, Stinton DP, Lowden RA, Anderson TJ, Starr TL. Recent advances in forced-flow, thermal-gradient CVI for refractory composites. *Surf Coatings Technol*. 1999;120–121:250-258.
7. Naslain R, Pallier R, Langlais F, Guette G, Jacques S. X-CVI (with X=I or P), A Unique Process for the Engineering and Infitration of the Interphase in SiC-Matrix Composites: An Overview. In: Zhang L, Jiang D, eds. *High Temperature Ceramic Composites 8, Ceramic Transactions Volume 248*, Westerville OH: American Ceramic Soc; 2014:391-301.
8. Zhou H, Singh RN. Processing and microstructural characterization of melt-infiltrated Si/SiC composites. *J Mater Synthesis Proc*. 1997;5:125-134.
9. Corman GS, Luthra KL. Silicon Melt Infiltrated Ceramic Composites (HiPerComp). In: Bansal NP, ed. *Handbook of Ceramic Composites*. Dordrecht, the Netherlands: Springer; 2005:99-115.
10. Morscher GN. Stress-dependent matrix cracking in 2D woven SiC-fiber reinforced melt-infiltrated SiC matrix composites. *Comp, Sci Technol*. 2004;64:1311-1319.
11. Morscher GN, Ojard G, Miller R, et al. Tensile creep and fatigue of Sylramic-iBN melt-infitrated matrix composites: retained properties, damage development, and failure mechanism. *Compos Sci Technol*. 2008;68:3305-3315.
12. Appleby MP, Zhu D, Morscher GN. Mechanical properties and real-time damage evaluations of environmental barrier coated SiC/SiC CMCs subjected to tensile loadings under thermal gradients. *Surf Coat Technol*. 2015;284:316-326.
13. Wing BL, EsmondeWhite F, Halloran JW. Microstress in reaction bonded SiC from crystallization expansion of silicon. *J Am Ceram Soc*. 99:3705-3711.
14. Hillig WB. Melt Infiltration Process for Making Ceramic Matrix Composites. In: Mazdiyasni KS, ed. *Fiber Reinforced Ceramic Composites*. Park Ridge, NJ: Noyes Publications; 1990:261-277.
15. Huang X, Wu K, Chen M, et al. Temperature dependence of Raman scattering in Si crystals with heavy B and/or Ge doping. *Mater Sci Semicond Process*. 2006;9:257-260.
16. Hart TR, Aggarwal RL, Lax B. Temperature dependence of Raman scattering in silicon. *Phy Rev B*. 1970;1:638-642.
17. Anastassakis E, Cantarero A, Cardona M. Piezo-Raman measurements and an harmonic parameters in silicon and diamond. *Phys Rev B*. 1990;41:7529-7535.
18. Xiao Z, Yang Y, Jin N, Liu S, Luo X, Huang B. Microstructure and thermal residual stress analysis of SiC fiber through Raman spectroscopy. *J Raman Spectroscopy*. 2013;44:1306-1311.
19. Olego D, Cardona M, Vogl P. Pressure dependence of the optical phonons and transverse effective charge in 3C-SiC. *Phys Rev B*. 1982;26:3878-3888.
20. DiGregorio JF, Furtak TE. Analysis of residual stress in 6H-SiC paricles within Al_2O_3/SiC composites through Raman spectroscopy. *J Am Ceram Soc*. 1992;75:1854-1857.
21. DiGregorio JF, Furtak TE, Petrovic JJ. A technique for measuring residual stress in SiC whiskers within an alumina matrix through Raman spectroscopy. *J Appl Phys*. 1992;71:3524-3531.
22. Huang X, Wu K, Chen M, et al. Temperature dependence of Raman scattering in Si crystals with heavy B and/or Ge doping. *Mater Sci Semicond Process*. 2006;9:257-260.
23. Stadelmann R, Lugovy M, Orlovskaya N, et al. Mechanical properties and residual stresses in ZrB_2 – SiC spark plasma sintered ceramic composites. *J Eur Ceram Soc*. 2016;36:1527-1537.
24. Esmonde-White FWL, Morris MD. Raman Imaging and Raman Mapping. In: Matousek P, Morris MD, eds. *Emerging Raman Applications and Techniques in Biomedical and Pharmaceutical Fields*. New York, NY: Springer-Verlag; 2010:97-110.
25. EsmondeWhite KA, EsmondeWhite FWL, Morris MD, Roessler BJ. Fiber-optic Raman spectroscopy of joint tissues. *Analyst*. 2011;136:1750-1785.
26. Wing BL. Residual stresses and oxidation of silicon carbide fiber reinforced silicon carbide composites, Ph.D. Dissertation. Ann Arbor, MI: University of Michigan; 2016.
27. Dunn D. The effect of fiber volume fraction in HiPerComp SiC-SiC, PhD Dissertation. Alfred NY: Alfred University; 2010.
28. Kingery WD. Note on thermal expansion and microstresses in two-phase compositions. *J Am Ceram Soc*. 1957;40:351-352.
29. Turner PS. Thermal-expansion stress in reinforced plastics. *J Res Natl Bur Standards*. 1946;37:230-250.
30. Munro RG. NIST materials properties databases for advanced ceramics. *Phys Chem Ref Data*. 1997;5:1195-1203.
31. Schall JD, Gao G, Harrison JA. Elastic constraints of silicon materials calculated as a function of temperature using a parameterization of the second-generation reactive empirical bond-order potential. *Phys Rev B*. 2008;77:115-209.
32. Gowayed Y, Ojard G, Santhosh U, Jefferson G. Modeling of crack density in ceramic matrix composites. *J Comp Mater*. 2015;49:2285-2294.

How to cite this article: Wing BL, Halloran JW. Microstress in the matrix of a melt-infiltrated SiC/SiC ceramic matrix composite. *J Am Ceram Soc*. 2017;100:5286–5294. https://doi.org/10.1111/jace.15038